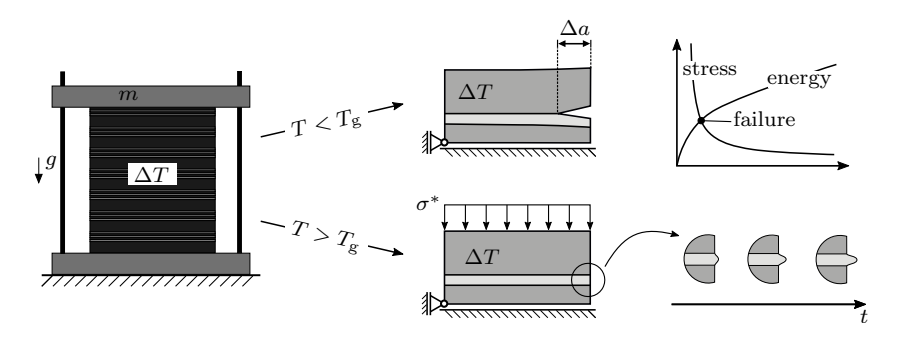
Graphical Abstract

A methodological contribution to failure prediction of glass ceramics sealings in high-temperature solid oxide fuel cell stacks

S. Bremm, S. Dölling, W. Becker, L. Blum, Ro. Peters, J. Malzbender, D. Stolten



Highlights

A methodological contribution to failure prediction of glass ceramics sealings in high-temperature solid oxide fuel cell stacks

- S. Bremm, S. Dölling, W. Becker, L. Blum, Ro. Peters, J. Malzbender, D. Stolten
 - Full three-dimensional model of an SOFC stack designed by Forschungszentrum Jülich
 - Identifying mechanical mechanisms in the context of high temperature sealing failure
 - Proposal of a methodology for the assessment of sealing failure in SOFC stacks
 - \bullet Coupled stress and energy criterion for $T < T_{\rm g}$
 - $\bullet~$ Viscoelastic considerations for $T>T_{\rm g}$

A methodological contribution to failure prediction of glass ceramics sealings in high-temperature solid oxide fuel cell stacks

S. Bremm^{a,*}, S. Dölling^a, W. Becker^a, L. Blum^b, Ro. Peters^b, J. Malzbender^b and D. Stolten^{b,c}

ARTICLE INFO

Keywords: High-temperature fuel cells Solid oxide fuel cells (SOFC) Glass ceramics sealant Sealing failure Finite fracture mechanics (FFM) Viscoelasticity

Abstract

Solid oxide fuel cells (SOFCs) provide electrical energy through a highly efficient direct transformation of chemical energy stored in fuels. The sealing between the stacked components of the SOFC has to prevent gas leakage towards the environment as well as mixing of fuel gas and oxidant in order to ensure a reliable long-term operability. Hence, the understanding of the sealing loading conditions and the failure assessment plays a major role regarding the improvement of current and future SOFC designs. In the present study, glass ceramics sealing failure is investigated by means of a current SOFC design. For this purpose, the stresses in the sealings are firstly examined by employing a fully parameterized three-dimensional finite element model. On the basis of a canonical example, the underlying physical mechanisms, which are responsible for the occurrence of stresses, are identified and their influence is discussed. Since the initiation of sealing failure is complex and depends on several parameters, a methodology for failure assessment is proposed. In this context, the glass transition temperature is of superordinate importance. Since the material properties differ significantly depending on whether the operating temperature is below or above the glass transition temperature, several competing failure mechanisms must be considered.

1. Introduction

Fuel cells appear to be a promising contribution to the technical solution of environmental problems such as global warming (Edwards et al. [1], Stambouli and Traversa [2]). Acting as electrochemical energy converters, they allow the efficient direct conversion of chemical energy, stored in a continuously fed gas or liquid fuel, into electrical energy. Hence, fuel cells are not limited to the Carnot efficiency, which is limiting the efficiency in conventional methods of providing energy through internal combustion engines.

There are different types of fuel cells but the basic structure is the same. The cell consists of two porous and thus permeable electrodes where the anode is in contact with the fuel and the cathode with the oxidant. The electrodes are separated by a selectively ion conducting electrolyte that is electrically insulating. Furthermore, the electrodes are connected via an external electric circuit. The electrons transferred during the electrochemical redox reaction flow through the external circuit and serve to provide electrical energy. In order to obtain a certain voltage, several cells can be combined and connected in an electrical series to a fuel cell stack. For further information, the interested reader is referred to Carrette et al. [3] and Ormerod [4].

Fuel cell types can be classified according to the used electrolytes as well as by their operating temperature. A widespread and widely developed type is the Proton Exchange Membrane Fuel Cell (PEMFC). It uses a proton

bremm@fsm.tu-darmstadt.de (S. Bremm)
ORCID(s): 0000-0002-7587-1762 (Ro. Peters)

exchange membrane as electrolyte and is classified as a low-temperature fuel cell (operating temperature 50–80 °C) yielding an electrical efficiency of 40–50% [2, 5]. The PEMFC exhibits a high power density, low operating temperatures and a quick response behavior to load changes (Mehta and Cooper [6]). Therefore, it is suitable for mobile applications such as spaceflight, automotive vehicles and portable power devices (Carrette et al. [3], Othman et al. [7]). However, the sound function of the electrodes requires noble metal catalysts such as platinum going along with high costs (Feng and Alonso-Vante [8]). Furthermore, the usually employed catalysts react sensitively to impurities (for instance carbon monoxide) that may be transported through the fuel gas yielding a catalyst poisoning that goes along with a significant reduction of efficiency (Cheng et al. [9]).

The Solid Oxide Fuel Cell (SOFC) is increasingly established as an alternative approach to the previously introduced PEMFC. As the operating temperature is in the range from about 600 °C to 1000 °C, SOFCs are often classified as high-temperature fuel cells. Since the operating temperature is determined by the electrolyte, typically yttria-stabilized zirconia is used as electrolyte [5, 10]. As a result, in contrast to PEMFCs, SOFCs do not contain noble metals [7]. Hence, the material costs are reduced significantly. Moreover, as key feature the SOFC can reach an energy conversion efficiency up to 65 % that is higher than that of the PEMFC [5, 10]. Due to the high operating temperature, a wide range of fuels may be processed [11]. Nevertheless, high operating temperatures result in slow startup/cool-down characteristics [11]. As a consequence, SOFCs are predestined for stationary applications such as electric power generating plants [12].

^aTechnical University of Darmstadt, Department of Mechanical Engineering, Institute of Structural Mechanics, 64287 Darmstadt, Germany

^bForschungszentrum Jülich GmbH, Institute of Energy and Climate Research (IEK), 52425 Jülich, Germany

^cRWTH Aachen University, Chair for Fuel Cells, Faculty of Mechanical Engineering, Kackertstr. 9, 52072 Aachen, Germany

^{*}Corresponding author

SOFC stacks may be differentiated according to their cell design [13]. The fuel cells may roughly be divided into planar and tubular designs. The designs differ, for instance, in regard to the power density, the sealing, and the fabrication. For further information about SOFC stack designs the reader is referred to Minh [12, 13] and Blum et al. [14]. Planar SOFC designs (pSOFCs) provide higher power densities than tubular SOFCs, but the sealings of the SOFC stack are more challenging [15, 16]. Since sealings are subjected to high operating temperatures, inhomogeneous temperature fields and an oxidizing atmosphere they are often life-limiting components. As even weak leakage may affect the cell performance [17], the development of sealings for SOFC applications has become a major challenge. For an overview of the development of seals we refer to Fergus [15], Mahapatra and Lu [16], Lessing [18].

The different proposed sealing concepts can be roughly divided into either rigid seals or compressible seals. Compressible seals consist of a compliant high-temperature material that is placed between the sealing surfaces and compressed by external forces on the fuel cell stack [18]. Since compressible seals are not materially bonded to the adjacent surfaces, they allow a relative movement between the involved surfaces. Hence, compressible seals can compensate different thermal expansion behavior of the SOFC components, for instance caused by different coefficients of thermal expansion (CTE) or inhomogeneous temperature fields, at least up to a certain point. However, as shown by numerous authors [15, 19-24] a hermetic sealing using compressible seals is not possible. Therefore, rigid seals, typically consisting of glasses or glass ceramics, are the most frequently used sealants for SOFC applications [16]. Due to rigidly bonded surfaces, leakage can be effectively avoided. In order to ensure proper SOFC operation, the rigid sealing has to meet several complex requirements. It has to withstand thermal stresses during operation induced by a mismatch in the coefficients of thermal expansion or inhomogeneous temperature fields, stresses due to the stack weight and gas pressure, cycles between room temperature and operating temperatures, creeping, and chemical reactions with the oxidizing atmosphere or the interfacing components [16]. At the same time, it has to be chemically stable, prevent electrical short circuits by an appropriate electrical resistivity, wet the sealing surfaces for a proper adhesion and ensure processability during manufacturing [16, 18].

Due to the high requirements, numerous studies were dedicated to the investigation of the mechanical and chemical properties of glass and glass ceramics sealants. Hence, only a choice of relevant works is introduced in the following. Smeacetto et al. [25] performed thermal cycling and aging experiments on glass ceramics sealants. Yang et al. [26], Batfalsky et al. [27] as well as Smeacetto et al. [28] investigated the chemical interaction between glass ceramics sealants and alloys. It has been revealed that sealants

containing barium aluminosilicate react with metallic interconnect at high temperatures yielding weak interfaces which are sensitive to interface cracking. The mechanical suitability of glass ceramics sealants for SOFC applications was investigated by Ley et al. [29] as well as Chang et al. [30]. They found that the operating temperature should be above the glass transition temperature of the glass ceramics in order to reduce stresses resulting from a CTE mismatch, taking viscosity into account. The viscoelastic properties of glass ceramics sealants were further investigated by several authors [31-33]. Lin et al. [34] found that stresses induced by a CTE mismatch may lead to a creep damage under high temperatures in the long-term run. There is strong evidence, that the glass ceramics sealing may be the critical component in the SOFC stack regardless of whether the operating temperature is above or below the glass transition temperature. The residual thermal stresses in the glass ceramics sealing result from differences in the CTE and inhomogeneous temperature fields which occur during the operation and while heating-up or cooling-down. Lin et al. [35] investigated thermal stresses in an SOFC stack under operating conditions as well as under ambient conditions using a three-dimensional finite element model. They observed highly inhomogeneous stress fields within the sealings but a failure prediction was only conducted using simple stress criteria. A coupled thermo-fluid-mechanical finite element analysis for an SOFC stack was performed by Peksen [36]. The sealing behavior in an SOFC stack was investigated experimentally as well as numerically by Blum et al. [37] under operating conditions for several glass ceramics sealants. Based on stress analyses different local design modifications were discussed in order to locally reduce stresses. In addition, Peksen [38] numerically examined stresses within the stack under non-steady state conditions.

Since the operating temperature is close to the glass transition temperature, there are parts of the seals below and parts above the glass transition temperature. With the glass transition temperature, the properties of the glass ceramics sealants also change significantly. Below that temperature, the glass ceramics behavior is brittle and above viscoelastic [31]. The change of material behavior must also be taken into account in the failure assessment. Below the glass transition temperature time invariant material behavior is expected. Since the stress fields are highly inhomogeneous especially at the free edges where they are theoretically infinite, a local stress criterion is not suitable. Alternatively, failure criteria based on linear elastic fracture mechanics (LEFM) were proposed. Such criteria require the existence of a pre-existing crack or an inherent flaw. Due to the lack of a defect, assumptions must be made regarding a fictitious defect size. In order to overcome these drawbacks, Leguillon [39] proposed a coupled stress and energy criterion within the framework of Finite Fracture Mechanics. It is assumed, that a crack of a certain length is formed instantaneously if both criteria are fulfilled simultaneously. The coupled criterion has been successfully applied to various structural

situations. For an overview the reader is referred to Weißgraeber et al. [40].

Above the glass transition temperature viscous effects have to be taken into account. On one hand viscous relaxation yields a reduction of interlaminar stresses in the glass ceramics sealing, induced for instance by a CTE mismatch, one the other hand viscous creeping goes along with large deformations. These large deformations may be problematic as cracks can occur as verified experimentally by Lin et al. [34]. Thus, viscous effects have to be taken into account in failure assessment, especially if failure occurs after some time in stationary operation.

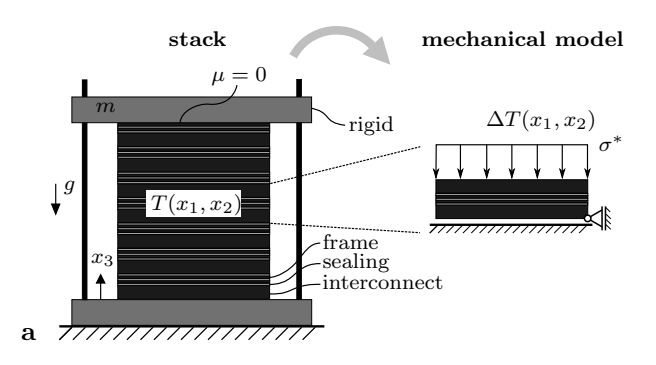
In the present study, a methodology for failure assessment in glass ceramics sealings is proposed. A current SOFC stack design, developed by Forschungszentrum Jülich, serves as a basis. Initially, the stresses within a glass ceramics sealing are investigated by means of a parameterized three-dimensional finite element model of a representative part of the SOFC stack. Subsequently, the different physical mechanisms inducing the stresses are examined. Therefore, a canonical model, capturing the physical effects, is introduced. After the investigation of the stresses, a methodology for their assessment is proposed. For this purpose, the glass transition temperature of the glass ceramics sealant serves as decision making parameter since the material behavior changes significantly by reaching this temperature. Both cases, above and below the glass transition temperature T_{σ} , are investigated since they occur simultaneously due to the inhomogeneous temperature field. A canonical model, related to the SOFC structural situation, is introduced in order to study both cases properly. Below $T_{\rm g}$ the material behaves brittle and the coupled stress and energy criterion within the framework of Finite Fracture Mechanics is employed in order to assess the highly inhomogeneous stress fields. Above T_{σ} viscous effects are considered and their influence on the stresses, resulting from different physical mechanisms, is studied. Finally, the achieved results are critically discussed.

2. 3D-Model

For the investigation of the (thermo-) mechanical aspects leading to sealing failure within high-temperature fuel cell stacks, first a full three-dimensional model of the considered SOFC stack is built and the resulting displacements and stresses are studied.

2.1. Mechanical Formulation

Starting point for this study is a fuel cell stack consisting of several periodically recurring repeating units as depicted in Fig. 1a on the left. Each repeating unit consists of one thick steel layer, which is the interconnect layer, and two additional thin steel frames. All steel layers are bonded by thin glass ceramics layers, serving as sealings. The stack is loaded by a mass m lying on top of it as well as a temperature field $T(x_1, x_2)$ caused by the operation of the stack, which is



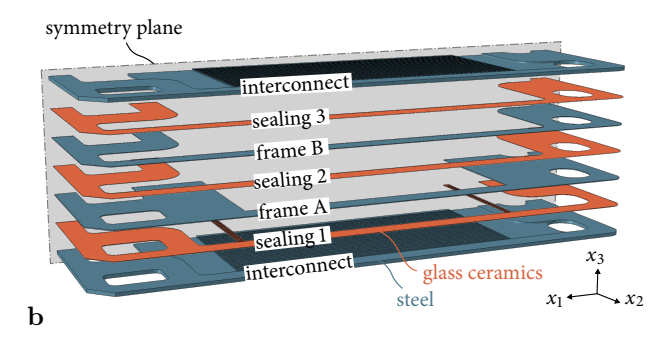


Figure 1: a Schematic representation of the fuel cell stack and the derived mechanical model. The model consists of one repeating unit of the stack, complemented by an additional interconnect layer, together with the boundary conditions shown above. b Layered structure of the modeled part of a fuel cell stack. One repeating unit consists of the layers interconnect (below) up to and including sealing 3. The modeled representative subunit contains an additional interconnect-layer.

assumed to be constant in x_3 -direction and depending only on the inplane coordinates x_1, x_2 .

Taking this into account, one representative subunit, as shown in Fig. 1a on the right, is modeled. The modeled subunit not only consists of one repeating unit, but an additional interconnect layer, assuming that this thick steel layer significantly influences the mechanical behavior. The boundary conditions for this mechanical model are: homogeneous displacement boundary conditions in x_3 -direction at the bottom, as well as one fixed node for the system to be statically determined and inhomogeneous stress boundary conditions $\sigma = \sigma^*$ at the top modeling the weight lying on the stack. In addition to that, a temperature load $\Delta T(x_1, x_2) = T(x_1, x_2) - T_0$ is imposed, where T_0 is the reference temperature at which the stack is assumed to be stressless.

2.2. Numerical Modeling

In order to determine the mechanical stress and to identify the resulting relevant physical mechanisms acting on the fuel cell stack, a full three-dimensional numerical model of the mechanical model presented in section 2.1 is implemented. For this purpose, the commercial finite element software ABAQUS, driven by a parameterized PYTHON script, is used. Figure 1b shows the structure and the geometries of the layers which are provided for the numeri-

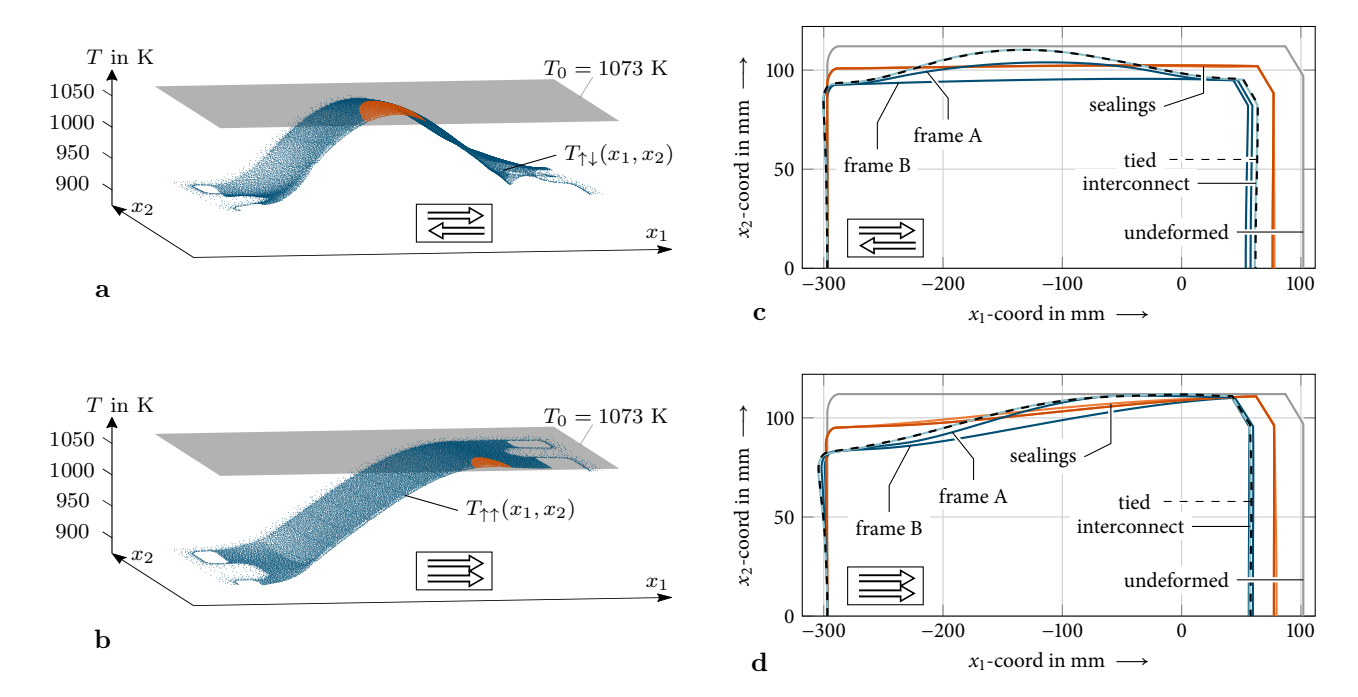


Figure 2: a,b Temperature fields (a) $T_{\uparrow\downarrow}(x_1,x_2)$ occurring during a counter gas flow and (b) $T_{\uparrow\uparrow}(x_1,x_2)$ during a parallel gas flow operation of the SOFC. These temperature fields are used as thermal load input for the finite element calculations. Temperatures higher than T_0 are marked in red, lower temperatures in blue. **c**,**d** Deformation of the outer boundaries of the layers of one repeating unit in a disassembled scenario and of the total repeating unit in a connected state. For the results shown in the upper picture (a), a counter gas flow operation and for the lower picture (b) a parallel gas flow operation of the SOFC is assumed. The deformations are scaled with a factor 100.

cal calculations. With regard to the computational effort, the shown symmetry property is taken into account allowing a half model. The reference temperature, where the stack is stressless is assumed as $T_0=1073\,\mathrm{K}$. The employed temperature fields shown in figure $2\mathbf{a}$, b arose from former computational fluid dynamics simulations performed by Forschungszentrum Jülich and represent two operation modes of an SOFC: A counter gas flow operation represented by the temperature field $T_{\uparrow\downarrow}(x_1,x_2)$ and a parallel gas flow operation represented by $T_{\uparrow\uparrow}(x_1,x_2)$. This leads to the load cases

$$\Delta T_{\uparrow\downarrow}(x_1, x_2) = T_{\uparrow\downarrow}(x_1, x_2) - T_0$$
 and
$$\Delta T_{\uparrow\uparrow}(x_1, x_2) = T_{\uparrow\uparrow}(x_1, x_2) - T_0.$$
 (1)

The mass of the weight lying on the top of the stack is $m = 800 \,\mathrm{kg}$, causing a prescribed compressive stress of $\sigma^* = 0.3 \,\mathrm{MPa}$. The material parameters employed for the steel as well as glass ceramics layers are listed in table 1. The data are taken from different literature sources, which are also indicated in the table.

2.3. Resulting Deformation and Stress Analyses

In order to get a first idea of the mechanical behavior of the modeled subunit, the deformations of the different layers under an inhomogeneous temperature load are analyzed. For this purpose, in a first step, each layer is separated, so that a free deformation independent from the other layers can take place. For this virtual thought experiment, we assume

Table 1Material parameters used for finite element calculations under the assumption that they are constant for the considered temperature range.

ν (-)	E (MPa)	$\alpha_{\rm T}$ (1/K)
	stee	
0.3 [41]	183 000 [42]	12×10^{-6} [42]
	glass ceramics	
0.3 [41]	87 000 [43]	9×10^{-6} [44]

 $\sigma^* = 0$. Then, the single layers are loaded with the temperature load (a) $\Delta T_{\uparrow\downarrow}(x_1, x_2)$, respectively (b) $\Delta T_{\uparrow\uparrow}(x_1, x_2)$. The free deformations of the outer boundaries of all layers are plotted in figure 2c,d in solid lines. Regarding these layer-wise deformations, two effects can be identified. First, the thermal expansion coefficients of steel and glass ceramics differ, more precisely $\alpha_{\rm T,st} > \alpha_{\rm T,gl}$ (see also table 1). This is why the magnitudes of the deformations of the steel layers are larger than those of the glass ceramics layers. Second, the inhomogeneous temperature field $T(x_1, x_2)$ has a different effect on the different layer geometries, so that the shape of the deformations is different for each layer. In comparison to that, the boundary deformation of a complete subunit, where all layers are connected, is plotted in a dashed line. As one can see, the deformation of the complete subunit almost coincides with the deformation of the interconnect,

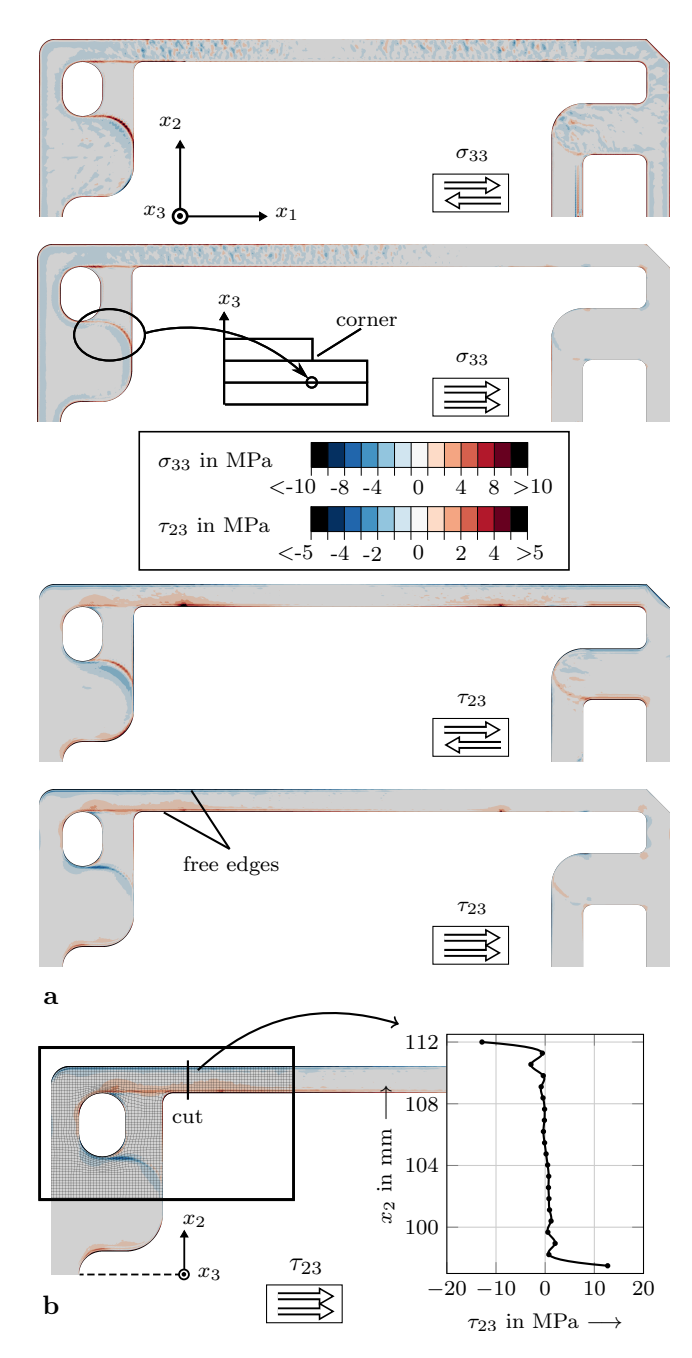


Figure 3: a Interlaminar normal stress σ_{33} and shear stress τ_{23} within a representative sealing (sealing 2) for counter as well as parallel gas flow operation. b Shear stress τ_{23} along a path defined by a virtual cut. Along x_2 a change of sign of τ_{23} can be seen. It is worth to mention that the peaks at the beginning and end will become larger when refining the mesh (singularity).

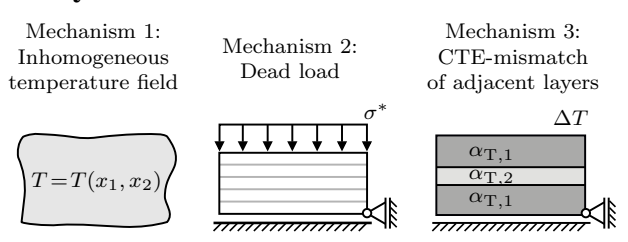
which is the stiffest layer, so that it dominates the deformation behavior of the total system.

Due to that, mechanical stresses occur within the layers, especially within the sealing, which may lead to premature sealing failure. In figure 3**a**, the failure relevant interlaminar

stresses τ_{23} and σ_{33} within a representative sealing are illustrated for counter as well as parallel gas flow operation. In both cases, the stress distribution is highly inhomogeneous. Dependent on the temperature load case, higher averaged stresses occur at the regions where the temperature difference is larger. This is in accordance with experiments performed by Forschungszentrum Jülich. They applied penetrating dye on a dummy stack in order to make cracks visible after disassembling the stack [37, 38]. Using this method, Blum et al. [37] showed that most of the leakage occurs at the side where the temperature difference is larger.

Furthermore, in figure 3**a**, stress concentrations can be observed at the free edges and at the location of corners which are present in the transition of layers with changing geometry. Figure 3**b** shows again the interlaminar shear stress τ_{23} exemplary for parallel gas flow operation. In order to get a more quantitative idea, the stresses are plotted for a certain path at a location where failure often is experimentally observed. For τ_{23} , a change of sign along x_2 can be seen. It is worth to mention that due to the singular character of τ_{23} , the peaks at the beginning and end of the path will become larger the finer the mesh.

3. Physical Mechanisms



Based on the deformation and stress analyses, resulting from the full three-dimensional model, three mechanical mechanisms can be identified playing a major role in the mechanical behavior of the fuel cell stack. First, the stack is loaded by an inhomogeneous temperature field $T(x_1, x_2)$. Due to the variability in x_1 and x_2 , the temperature field induces thermal stresses within the layers in the x_1 - x_2 -plane, since no uniform expansion or contraction can take place. This can also be seen in figure 2c,d. The separated layers exhibit different deformation shapes, because the inhomogeneous temperature field affects the different layer geometries in different ways. The inhomogeneous temperature field itself leads to stresses and since the layers are connected, additional stresses are caused. Second, the stack is loaded by a weight applied on the top, which is modeled by a prescribed stress σ^* . Due to that, mechanical compression stresses arise within the stack. Assuming a linear-elastic material behavior, this mechanism also will cause interlaminar shear stresses if the Poisson's ratio ν of adjacent layers differs. In addition to that, this mechanism plays a major role when assuming a viscoelastic material behavior, which will be further shown in section 4. The third mechanism occurs assuming different thermal expansion coefficients of adjacent layers $\alpha_{T,1} \neq \alpha_{T,2}$. For the fuel cell stack considered in

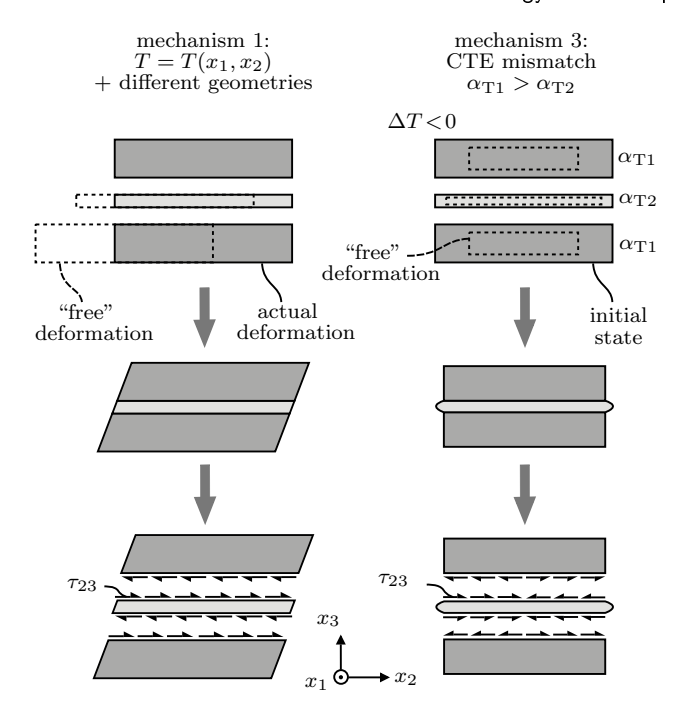


Figure 4: Mechanism 1 (inhomogeneous temperature field), combined with different layer geometries leads to a displacement of the layers relative to one another (see also figure $2\mathbf{c},\mathbf{d}$). This mechanism results in a stress τ_{23} with no change of sign (left column). Mechanisms 3 (mismatch in coefficients of thermal expansion in adjacent layers) results in a stress curve τ_{23} with change of sign along x_2 . Assuming a mismatch in Poisson's ratios ($v_1 \neq v_2$), mechanism 2 (dead load) also induces a change of sign of τ_{23} (without illustration).

section 2, it is $\alpha_{T,st} > \alpha_{T,gl}$ as shown in table 1. Here, assuming a cooling ($\Delta T < 0$), the steel layers strive to contract more than the glass ceramics layers. But since the layers are connected, they cannot deform independently, so that shear stresses at the interfaces of the steel and glass ceramics layers have to be expected.

In figure 4, the effect of the mentioned mechanisms on the failure relevant interlaminar shear stress τ_{23} is illustrated by means of a two-dimensional representative section. In the first column mechanism 1 is depicted, which is the inhomogeneous temperature field combined with different layer geometries. Assuming a virtual separation of the layers, this mechanism will lead to a relative displacement of the layers (see also figure 2**c,d**). This, in a state where the layers are connected, leads to an interlaminar stress τ_{23} , which has no change of sign along x_2 . The second column shows the effect of the mechanisms 2 and 3 on τ_{23} , which is exemplarily shown for mechanism 3, i.e. mismatch of thermal expansion coefficients. Assuming a free, independent deformation under a negative temperature load $\Delta T < 0$ and layers with $\alpha_{\rm T1} > \alpha_{\rm T2}$, the $\alpha_{\rm T1}$ -layers would contract more than the α_{T2} -layer. Since the layers are connected, they constrain each other. More specifically, the α_{T1} -layers cannot contract as much and the α_{T2} -layer has to contract more as it would if

it could deform freely. This leads to a shear stress τ_{23} with a change of sign along x_2 . For the sake of completeness it should be mentioned that if the Poisson's ratio of the layers differs, $v_1 \neq v_2$, mechanism 2 will have the same effect on the sign of the shear stress τ_{23} (without illustration). Consequently for mechanism 3 (and 2 if $v_1 \neq v_2$), the sign of τ_{23} changes along x_2 , whereas for mechanism 1 it does not. This can be used as an indicator in order to determine which of these mechanisms dominates the mechanical behavior of the considered system.

According to section 2.3, a change of sign of τ_{23} is observed exemplarily for parallel gas flow operation in a representative path at a critical location. For the fuel cell stack considered in section 2, the Poisson's ratios of steel and glass ceramics are equal ($v_{\rm st} = v_{\rm gl}$, see table 1). This indicates that mechanism 3 is dominating for the linear elastic case.

4. Methodology for the Assessment of Sealing Failure

Previously, the stresses and resulting physical mechanisms were considered for the linear elastic case. However, for the evaluation of sealing failure, a further step is necessary. In the following, a methodology for the assessment of glass ceramics sealings failure, as they occur for example in SOFC stacks, is proposed. According to figure 5, for the failure assessment, several influence factors have to be taken into account. Due to the operation of the fuel cells with oxygen, corrosion effects may appear, which has been investigated by several authors [18, 26, 27]. In addition to that, the SOFC stack is exposed to different operation cases during its lifetime. On the one hand, a quasistatic stationary operation and on the other hand, a cyclic loading resulting from starting and cooling down the fuel cell may be considered. In the following, the former operation case is considered, whereas the effects of thermal cycling are for example addressed by Smeacetto et al. [25].

SOFCs typically operate at temperatures around the glass transition temperature T_g . According to experiments by Osipova et al. [45], the glass transition temperature for SOFC sealants is roughly around $T_g \approx 970 \,\mathrm{K}$. As can be seen in figure 2a,b, within the considered SOFC sealing, there are areas above as well as areas below this temperature. Unfortunately, the material behavior of the glass ceramics strongly depends on whether the operating temperature is above or below the glass transition temperature. Consequently, within the failure assessment a distinction of cases concerning the operating temperature of the SOFC has to be made. In regions below the glass transition temperature, $T < T_g$, the glass ceramics behaves brittle, so that methods for the assessment of brittle failure have to be applied, which is described detailed in section 4.1. Above the glass transition temperature, $T > T_g$, viscous material behavior occurs, which is explained in section 4.2 in more detail.

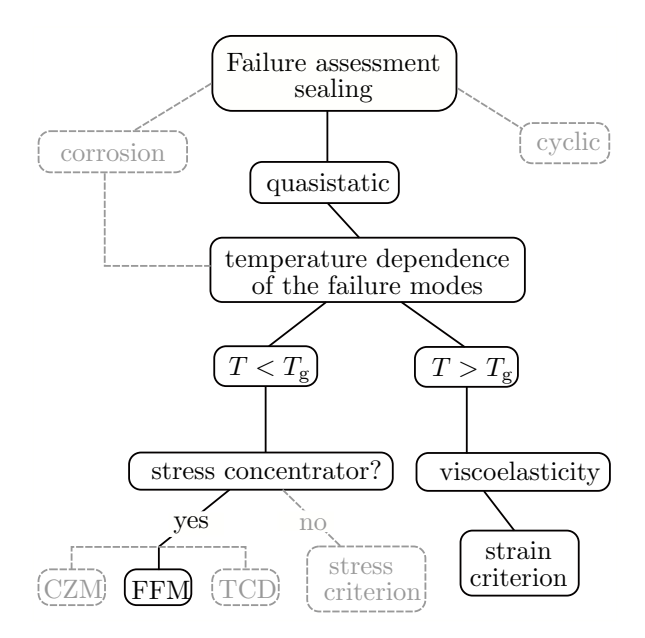


Figure 5: Methodology for the assessment of class ceramic sealings within SOFC stacks. Used abbreviations: $T_{\rm g}$ glass transition temperature, CZM Cohesive Zone Modeling, FFM Finite Fracture Mechanics, TCD Theory of Critical Distances.

4.1. Failure Assessment for $T < T_g$: Brittle Material Behavior

The stress fields within the sealings of the SOFC stack shown in section 2.3 are highly inhomogeneous, especially at the free edges, where stress concentrations were observed. This is a well-known effect, which occurs in laminates due to the elastic mismatch of adjacent plies and causes weak stress singularities as shown by Hein and Erdogan [46]. It is called the free-edge effect (see also Kant and Swaminathan [47], Mittelstedt and Becker [48, 49]). Classical stress-based failure hypotheses cannot be applied directly to structural situations with stress singularities. Because of the theoretically infinite stresses at the free edge, a classical stress criterion would be fulfilled immediately already for arbitrary small loads. On the other hand, energy-based criteria which are used in classical Linear Elastic Fracture Mechanics (LEFM), i.e. the Griffith's criterion, can only be applied on strong stress singularities as they appear at crack tips. For weak singularities, the differential energy release rate becomes zero so that the energy criterion would never be fulfilled independently of the load. This is why a pre-existing crack or inherent flaw has to be assumed using LEFM-based criteria (Waddoups et al. [50], Leblond and Mouro [51, 52]). A common approach in order to make the stress criterion applicable for weak singularities is to evaluate it a certain distance away from the stress concentration, which was for example employed by Neuber [53], Whitney and Nuismer [54]. This non-local approach more recently has been reformulated as the Theory of Critical Distances (TCD) as proposed by Taylor [55]. The drawback of these methods is the need of a length parameter, which is not known a priori. This parameter not only depends on the material but

also on the given geometry (e.g. Dunn et al. [56], Qian and Akisanya [57]), so it has to be determined for every structural situation for example by experiments. An alternative approach for the treatment of brittle failure at arbitrary stress raisers is the Cohesive Zone Model (CZM), which is based on damage mechanics and whose origins go back to Barenblatt [58] and Dugdale [59]. However, it requires the definition of an appropriate traction-separation law and leads to nonlinear problems with high computational efforts.

Beyond the described approaches, Hashin [60] postulated the instantaneous formation of finite sized cracks ("crack events") and referred to this as Finite Fracture Mechanics (FFM). Using that framework, Leguillon [39] proposes a coupled energy and stress criterion for the assessment of brittle failure. It states that two necessary conditions have to be fulfilled simultaneously: a stress and an energy criterion. Due to the non-local approach of the criteria, this method can be applied on weak singularities as they occur for instance at the free edge of bi-material junctions (see for example Martin et al. [61] and Dölling et al. [62]). Evaluating the coupled criterion requires only solving linear problems, which makes the method more efficient than for example CZM. Furthermore it requires only the material properties strength and toughness. The coupled criterion leads to a minimization problem which provides the critical load as well as the corresponding crack length.

There are various approaches for the formulation of the stress and energy criterion needed for the coupled criterion. Here, for the glass ceramics sealings, the stress criterion is assumed as an interaction relation with exponent $n_f \in \mathbb{N}$, which has to be chosen appropriately:

$$f\left(\sigma(x, \Delta T)\right) = \left(\frac{\left\langle\sigma_{yy}\right\rangle}{\sigma_{yy,c}}\right)^{n_{\rm f}} + \left(\frac{\left|\tau_{xy}\right|}{\tau_{xy,c}}\right)^{n_{\rm f}},\tag{2}$$

where $\langle \cdot \rangle$ denote the Macaulay brackets. This interaction relation is a common choice which has already been employed successfully by various authors [63–66], especially for brittle interfaces. The coordinates $\mathbf{x} = (x, y)$ refer to the coordinate system introduced in figure $7\mathbf{a}$, σ is the stress tensor and σ_{yy} and τ_{xy} some of its components, more precisely the normal stress in y-direction and the shear stress. Furthermore, $\sigma_{yy,c}$ and $\tau_{xy,c}$ are the tensile, respectively shear strength. In order to provide a non-local criterion, (2) is declared to be fulfilled if

$$f(\sigma(\mathbf{x}, \Delta T)) \ge 1 \quad \forall \mathbf{x} \in \Gamma(\Delta a),$$
 (3)

where $\Gamma(\Delta a) \subset \Omega_u$ is the subset of coordinates of the uncracked domain Ω_u , where the potential crack of length Δa will occur, see figure $7\mathbf{a}$ on the left.

For the energy criterion, a similar interaction relation with exponent $n_g \in \mathbb{N}$ is assumed as it has been done for example by Tran et al. [66], Wu and Reuter Jr. [67], Reeder

[68]:

$$g\left(\overline{\mathcal{G}}(\Delta a, \Delta T)\right) = \left(\frac{\overline{\mathcal{G}}_{\rm I}}{\mathcal{G}_{\rm I,c}}\right)^{n_{\rm g}} + \left(\frac{\overline{\mathcal{G}}_{\rm II}}{\mathcal{G}_{\rm II,c}}\right)^{n_{\rm g}},\tag{4}$$

where $\mathcal{G}_{I,c}$ and $\mathcal{G}_{II,c}$ are the mode I and II fracture toughnesses of the material. Moreover, $\overline{\mathcal{G}} = (\overline{\mathcal{G}}_I, \overline{\mathcal{G}}_{II})$ are the incremental energy release rates for the crack opening modes I and II, gathered in a vector. They can be written as

$$\overline{\mathcal{G}}_i(\Delta a, \Delta T) = -\frac{\Delta \Pi_i}{\Delta a} = \frac{1}{\Delta a} \int_0^{\Delta a} \mathcal{G}_i(a, \Delta T) \, \mathrm{d}a, \quad (5)$$

 $i \in \{\mathrm{I}, \mathrm{II}\}$, where $-\Delta\Pi_{\mathrm{II}}$ or $-\Delta\Pi_{\mathrm{II}}$ is the potential energy change between the uncracked and cracked states concerning mode I or II. The right equation describes the incremental energy release rates $\overline{G}_{\mathrm{I}}$ and $\overline{G}_{\mathrm{II}}$ as the differential energy release rates G_{II} and G_{II} averaged over the finite crack of length Δa . The criterion (4) is declared to be fulfilled for

$$g\left(\overline{\mathcal{G}}(\Delta a, \Delta T)\right) \ge 1.$$
 (6)

According to the coupled stress and energy criterion, both criteria have to be fulfilled simultaneously for an initiation of a crack. For the determination of the failure load (which in our case is the critical temperature change $|\Delta T_{\rm f}|$), the coupled stress and energy criterion yields the following optimization problem

$$|\Delta T_{\rm f}| = \min \{ |\Delta T| : \exists \Delta a > 0 \text{ with}$$

$$f(\sigma(\mathbf{x}, \Delta T)) \ge 1 \ \forall \mathbf{x} \in \Gamma(\Delta a)$$

$$\wedge \ g(\overline{\mathcal{G}}(\Delta a, \Delta T)) \ge 1 \ \}.$$
(7)

Consequently, the failure temperature change $|\Delta T_{\rm f}|$ is the minimal temperature change where both, stress and energy criterion, are fulfilled. The corresponding initiated crack length $\Delta a_{\rm f}$ is a priori unknown and can be determined while solving the optimization problem.

4.2. Failure Assessment for $T > T_g$: Viscoelastic Material Behavior

For a temperature above the glass transition temperature, $T > T_{\rm g}$, glass ceramics behaves viscoelastic. This behavior within the scope of SOFC sealings is investigated by several authors [31–34, 69–72].

The material law for isotropic linear elastic material reads:

$$\operatorname{tr}(\boldsymbol{\sigma}) = 3K \operatorname{tr}(\boldsymbol{\varepsilon})$$

 $\operatorname{dev}(\boldsymbol{\sigma}) = 2G \operatorname{dev}(\boldsymbol{\varepsilon})$ (8)

with $\operatorname{\mathbf{dev}}: \mathbb{R}^{n\times n} \to \mathbb{R}^{n\times n}, \operatorname{\mathbf{dev}}(\mathbf{M}) := \mathbf{M} - \frac{1}{3}\mathrm{tr}(\mathbf{M})\mathbf{I},$ where \mathbf{I} is the identity. Here, $\boldsymbol{\varepsilon}$ is the strain and $\boldsymbol{\sigma}$ the stress tensor. The material law is represented in terms of the bulk modulus K and shear modulus G. Reformulation of (8) yields

$$\varepsilon = \frac{1}{2G}\sigma + \left(\frac{1}{9K} - \frac{1}{6G}\right)\operatorname{tr}(\sigma)\mathbf{I} \tag{9}$$

For the viscoelastic material behavior of glass ceramics, the following assumptions are made: the bulk modulus K is assumed to behave linear elastic, whereas the shear modulus G may exhibit a viscoelastic material behavior. This yields

$$K = \frac{E}{3(1-2\nu)} = \text{const.},$$

 $G = G(t) \text{ with } G_0 = G(t=0) = \frac{E}{2(1+\nu)}$ (10)

Assuming a uni-axial tension test in \tilde{x}_3 -direction, where the strain $\tilde{\varepsilon}_{33}(t)$ is measured as a function of time, the shear relaxation G(t) can be expressed as



$$G(t) = \left(\frac{3\,\tilde{\varepsilon}_{33}(t)}{\sigma_0} - \frac{1}{3\,K}\right)^{-1} \tag{11}$$

Due to its declining character, G(t) may be described by a series of exponential functions, the so-called *Prony series*

$$G(t) = G_{\infty} + \sum_{i=1}^{n} G_i e^{-t/\tau_i}$$
 (12)

where G_{∞} represents the long-term shear modulus and the coefficients G_i and τ_i characterize the material behavior. The coefficients G_i are often normalized using

$$g_i = \frac{G_i}{G_0},\tag{13}$$

where $G_0 = G_{\infty} + \sum_{i=1}^{n} G_i$ is the instantaneous shear modulus. For given experimental data the coefficients can be adjusted by a regression analysis.

5. Exemplary Application of the Methodology

In the following, the methodology for the assessment of sealing failure described above is applied to a simplified representative model. The employed boundary value problem is depicted in figure 6. Since the three-dimensional model (fig. 1b), on which the simplified representative model (fig. 6) is based, has a sufficiently large extension in x_1 -direction, only a virtual cross section in the x_2 - x_3 -plane is regarded further assuming a plane strain state. Therefore a new coordinate-system (x, y) is introduced. The model consists of one glass ceramics layer which is between two steel layers. It is supported statically determined and loaded by a pressure load σ^* as well as thermal load ΔT . The geometrical dimensions are based on those of the respective layers within SOFC stacks and are listed in table 2.

Table 2 Geometry data.

<i>l</i> in mm	h in mm	t ₁ in mm	t ₂ in mm
14.5	0.125	0.3	2.5

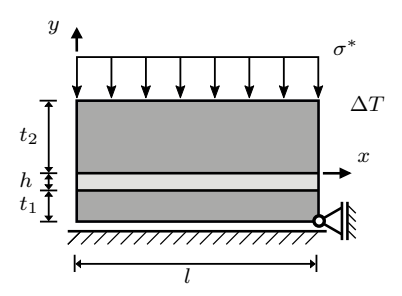


Figure 6: Representative plane strain submodel for the investigation of the physical mechanisms acting on a fuel cell stack using the presented methodology.

5.1. Results Finite Fracture Mechanics for $T < T_{o}$

For the application of the coupled criterion (7), the exponents in the stress (2) and energy (4) criteria are set to $n_{\rm f}=2$, which is a common choice used for example by Brewer and Lagace [63] and Tran et al. [66] and $n_{\rm g}=1$ (e.g. Tran et al. [66], Stein et al. [73]). This yields a quadratic interaction relation for the stress and a linear interaction relation for the energy criterion.

Due to the experimental results of Stephens et al. [32], it is assumed that the tensile strength of the glass ceramics can roughly be set to twice the shear strength, $\sigma_{yy,c} = 2\,\tau_{xy,c}$. Furthermore, it is assumed that $G_{\rm II,c} = 2\,G_{\rm I,c}$, which is a common simplifying assumption (see Stein et al. [73], da Silva et al. [74], Campilho et al. [75], Jung Lee et al. [76]). Hence, only two fracture parameters are required for the formulation of the coupled criterion.

For the investigation of brittle failure, the pressure load σ^* illustrated in figure 6 is neglected, $\sigma^*=0$. This yields a conservative estimation, since mechanism 2 (dead load) would counteract crack growth assuming a linear elastic material behavior. Consequently, this study represents mechanism 3 (mismatch in thermal expansion coefficients α_T), which is according to the sections 2.3 and 3 the dominating mechanism for the linear elastic case.

In the present case, it is assumed that the crack emanates at the origin of the coordinate system (which is also the origin of the stress concentrator) and follows the x-axis (which coincides with the material interface), so that

$$\Gamma(\Delta a) = \{(x,y) \in \Omega_{\mathrm{u}} \ \colon x \in [0,\Delta a], y = 0\}.$$

Zhao et al. [43] experimentally determined fracture toughnesses $K_{\rm I,c}$ of glass ceramics sealants for SOFCs. According to these experiments using $\mathcal{G}_{\rm I,c}=(1-v^2)\,K_{\rm I,c}^2/E$ with v=0.3, $\mathcal{G}_{\rm I,c}$ lies in the interval

$$G_{I,c} \in [0.0028, 0.0398] \frac{N}{mm}$$
 (14)

This interval also includes the experimental data from Abdoli et al. [77]. Furthermore, the data from Malzbender et al. [78, 79] confirm the order of magnitude of the stated fracture toughnesses. In a torsion test, Osipova et al. [45] measured

shear strengths

$$\tau_{xy,c} \in [14.0, 68.6] \text{ MPa}$$
 (15)

for sealing glass ceramics. The test results of Stephens et al. [32] are also in this range.

In figure 7b, the coupled stress and energy criterion is illustrated for exemplary material data within the intervals (14) and (15). In dashed lines, the stress criterion (2) is plotted for different temperature loads $|\Delta T|$. The criterion is fulfilled if f is larger than one in the whole x-range zero to Δa :

$$f(\sigma((x,0),\Delta T)) \ge 1 \ \forall x \in [0,\Delta a].$$

In solid lines, the energy criterion (4) is plotted for different temperature loads $|\Delta T|$. The criterion is satisfied for the crack lengths Δa for which g is larger than one (see equation (6)).

For $|\Delta T|=600\,\mathrm{K}$, there is no Δa for which both criteria are fulfilled simultaneously. Thus, the coupled criterion postulates no initiation of a crack for this temperature change. On the other hand, for $|\Delta T|=900\,\mathrm{K}$, both criteria are fulfilled for more than one Δa , so that the coupled criterion predicts failure. The smallest load at which a Δa (= $\Delta a_{\rm f}$) exists for which both criteria are fulfilled simultaneously, so that crack initiation is expected, is the failure load $|\Delta T_{\rm f}|=767\,\mathrm{K}$. The corresponding finite length of the initiated crack is $\Delta a_{\rm f}=0.144\,\mathrm{mm}$. This crack length is in the same order of magnitude as the respective adhesive layer thickness h.

In the following, the influence of the failure relevant material parameters on the macroscopic failure behavior is investigated. Therefore, a sensitivity analysis concerning strength and toughness of the sealing material is performed. In figure 7**c,d**, the absolute value of the failure load $|\Delta T_f|$ is plotted (a) over the shear strength $\tau_{xy,c}$ for exemplary fracture toughnesses $\mathcal{G}_{\text{L,c}}$ and (b) over the fracture toughness $\mathcal{G}_{\text{L,c}}$ for exemplary shear strengths $\tau_{xy,c}$. Both failure relevant parameters are varied within the ranges (14) and (15). It can be seen from both of these figures that the failure load strongly depends on the fracture toughness $\mathcal{G}_{I,c}$. With regard to the shear strength $\tau_{xy,c}$, only a slight dependence can be observed, especially for higher fracture toughnesses. Thus, most of all the correct value of the fracture toughness \mathcal{G}_{Lc} is relevant. It is the significant parameter and has to be determined properly in order to achieve a reliable result concerning the failure load.

5.2. Results Viscoelastic Model for $T > T_{o}$

In order to investigate the viscoelastic behavior of the glass ceramics sealing, first the time-dependent behavior of the shear modulus G(t) of the glass ceramics material has to be determined. For this purpose, experimental data obtained by Abdoli et al. [69] are exemplarily taken into account, where the time-dependent creep strain $\varepsilon_{cr}(t)$ =

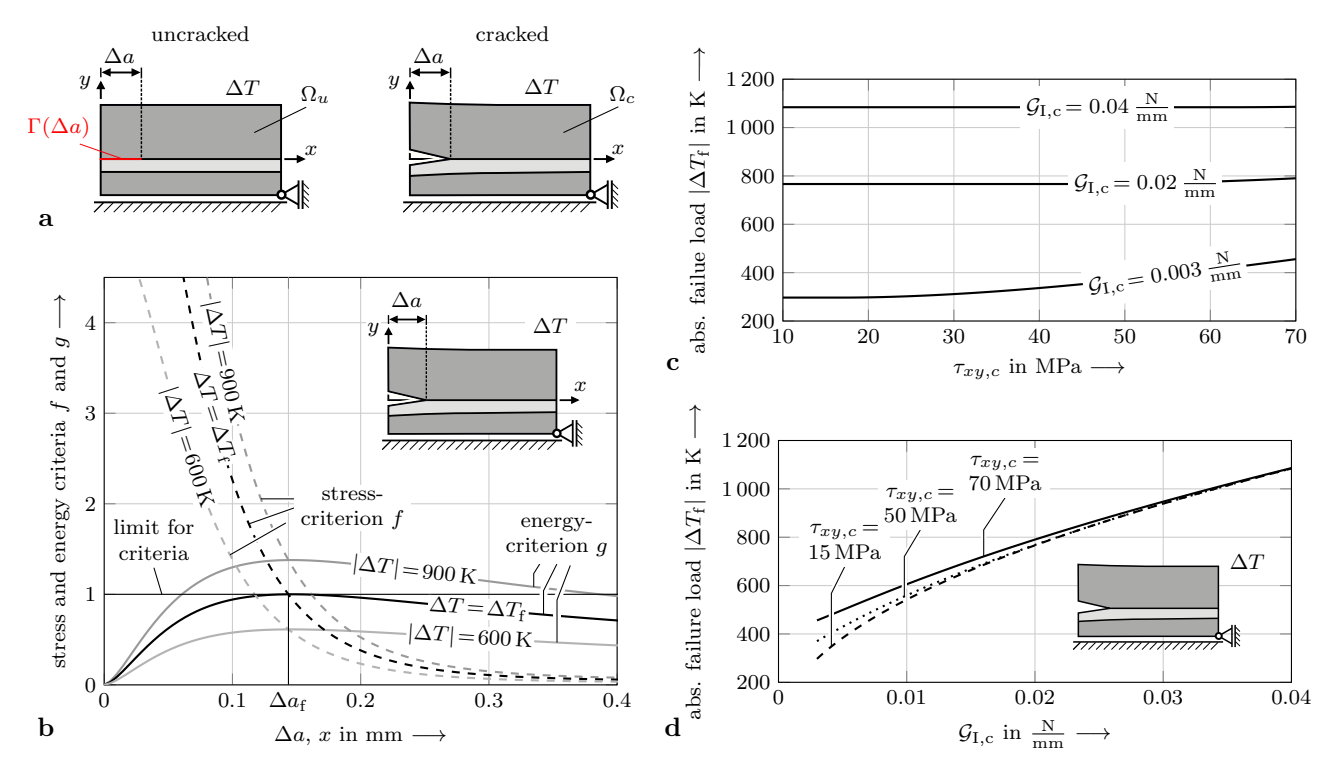


Figure 7: a Uncracked and cracked domain $\Omega_{\rm u}$ and $\Omega_{\rm c}$ of a minimal thermal example on which the Finite Fracture Mechanics is explained. b Energy and stress criteria for failure prediction using failure-related parameters $\mathcal{G}_{\rm I,c}=0.02\,\mathrm{N/mm}$ and $\tau_{xy,c}=45\,\mathrm{MPa}$. The criteria are plotted for different loads $|\Delta T|$, including the failure load $|\Delta T_{\rm f}|=767\,\mathrm{K}$. c,d Absolute value of the failure load $|\Delta T_{\rm f}|$ determined with the help of the coupled stress and energy criterion and plotted for various shear strengths $\tau_{xy,c}$ and fracture toughnesses $\mathcal{G}_{\rm I,c}$, where it is assumed that $\sigma_{yy,c}=2\,\tau_{xy,c}$ and $\mathcal{G}_{\rm II,c}=2\,\mathcal{G}_{\rm I,c}$.

Table 3 Prony series coefficients resulting from a least-squares fit, n=4.

i	1	2	3	4
$\overline{\tau_i}$	$10^{1} \mathrm{s}$	$10^{2} \mathrm{s}$	$10^{3} \mathrm{s}$	10 ⁴ s
g_i	0.8514	0.1316	0.0099	0.0070

 $\tilde{\varepsilon}_{33}(t) - \tilde{\varepsilon}_{33}(t=0)$ is specified. These data are illustrated together with the back-calculation of the shear relaxation (11) in figure 8a. The recalculated data are fitted to a Prony series (12) using a least-squares fit yielding the coefficients given in table 3. Using the representative submodel shown in figure 6, together with the viscoelastic glass ceramics sealing properties represented by the Prony series coefficients in table 3, time-dependent viscoelastic finite element calculations are performed. For the investigation of the time-dependent behavior of the physical mechanisms identified in section 3, three different load cases are considered: only the dead load σ^* , only the temperature change ΔT and both combined. The value of $\sigma^* = 0.3$ MPa is the same as used for the full three-dimensional model in section 2 and the order of magnitude of the temperature load $\Delta T = 200 \,\mathrm{K}$ is similar to the maximal occurring temperature difference in operation of the SOFC (see also figure 2**a,b**).

The resulting relative displacements $u_{\text{rel}} = |u_{x,\text{adve}} - u_{x,\text{adnd}}|$ between adhesive and adherend are shown in figure $8\mathbf{b}$

For a loading only by the temperature change $\Delta T \neq 0$ (dotted line), there is an initial relative displacement of adhesive and adherend resulting from the mismatch in the thermal expansion coefficients of the two materials (mechanism 3). The relative displacement u_{rel} is reduced over time, which is initially to be assessed positively. If the model is loaded by nothing but the pressure load (mechanism 2) $\sigma^* \neq 0$ (dashed line), the relative displacement $u_{\rm rel}$ increases monotonically over the time. Consequently, in long-term operation, the dead load σ^* leads to very large deformations within the glass ceramics, which may reach a critical size. For a loading of the model with both, temperature load $\Delta T \neq 0$ and pressure load $\sigma^* \neq 0$ (solid line), both observed effects are superimposed. After an initial displacement $u_{rel}(t=0)$, the relative displacement first decreases, similar to the ΔT -load case. After a time of around $t = 10^3$ s, the effect of σ^* seems to preponderate, such that the relative displacement u_{rel} gets dominant and keeps increasing. Thus, for this combined load case, also very large deformations within the glass ceramics have to be expected after a certain time. It is worth to mention that in the real stack assembly there is not only the sealing area but also the electrical contact via cell and adjacent layers which at

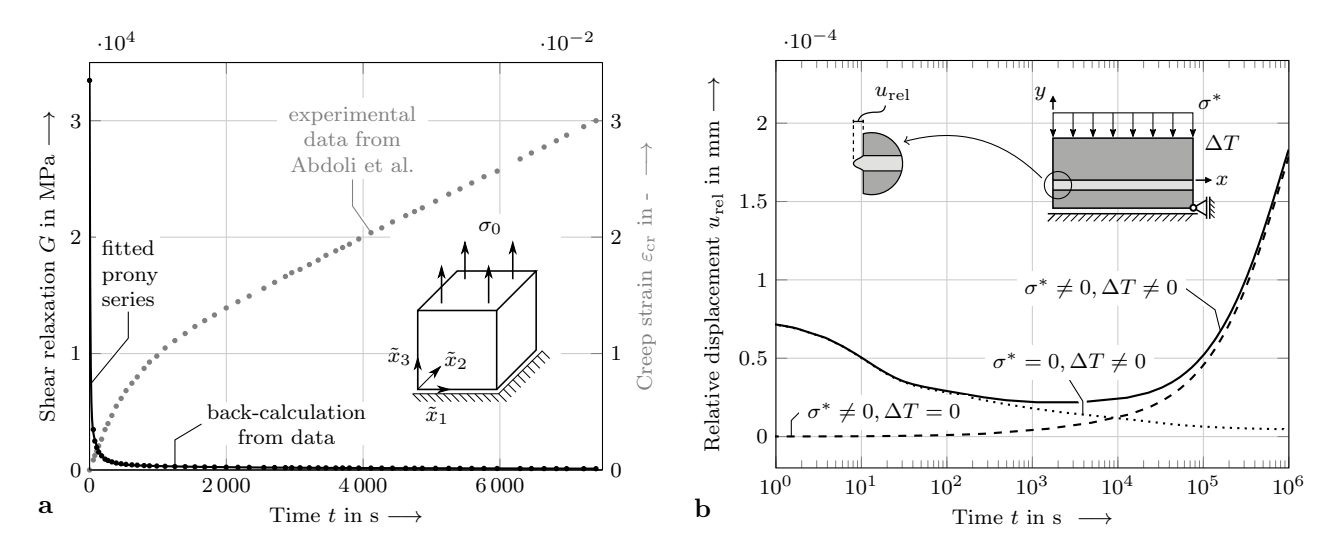


Figure 8: a Experimental data for creep strain $\varepsilon_{\rm cr}(t)=\tilde{\varepsilon}_{33}(t)-\tilde{\varepsilon}_{33}(t=0)$ from Abdoli et al. [69] with $\sigma_0=10\,{\rm MPa}$ and back-calculated shear relaxation G(t). For fitting the coefficients of the Prony series, a least squares approximation is performed. b Relative displacement $u_{\rm rel}=|u_{x,\rm adne}-u_{x,\rm adnd}|$ between adhesive and adherend over time for a 2D representative model in viscoelastic calculations with and without pressure load $\sigma^*=0.3\,{\rm MPa}$ and without temperature load $\Delta T=200\,{\rm K}$.

least take a part of the load σ^* . Although this behavior is not captured by the canonical model, it still yields reliable results as long as the load carried by the cell is sufficiently small.

Furthermore, it is expected that there also can be time-dependent effects resulting from the inhomogeneous temperature field (mechanism 1) assuming viscoelastic material behavior. In a long-term behavior, the frames are assumed to adjust just as in the disassembled scenario in figure 2c,d. Due to the relative displacement of the frames, shear deformations can occur in the glass ceramics, which might even reach and exceed a critical value.

6. Additional applications and improvements

Starting point for the present study was the SOFC stack designed by *Forschungszentrum Jülich*. Using the introduced two-dimensional representative model, the results of the present analysis are transferable to other SOFC stacks. Furthermore, the developed methodology is applicable to various layered structures using glass ceramics under a temperature load above and below its glass transition temperature.

Having the two-dimensional model, together with the derived physical mechanisms and the assessment of sealing failure in hand, different strategies for an improvement of the sealing joint can be derived. First, it is desirable to design the involved materials such that the coefficients of thermal expansion are as close as possible, here $\alpha_{T,st} \approx \alpha_{T,gl}$. Assuming a brittle material behavior, the failure relevant material parameters of the glass ceramics, i.e. the strengths $\tau_{xy,c}, \sigma_{yy,c}$, but especially the fracture toughnesses $\mathcal{G}_{I,c}, \mathcal{G}_{II,c}$ should be preferably high. Further applications of the cou-

pled criterion, which are not shown in this work, reveal that it is advantageous to design the sealing joint geometry such that the sealing is as thin as possible yielding a higher failure temperature load $|\Delta T_{\rm f}|$. This thickness effect is well-known in the field of adhesively bonded structures and has been shown by various authors, for example [74, 80–82].

Among others, Ley et al. [29] and Chang et al. [30] suggest to operate the fuel cell stack at a temperature $T > T_{\rm g}$ in order to take advantage of stress relaxation effects within the glass-ceramics. This can provide a better tolerance of a CTE mismatch. However, besides a stress relaxation, viscoelastic material behavior also leads to very large deformations which may lead to sealing failure (see section 5.2). In order to avoid this, the operation temperature of the stack has to be below the glass transition temperature, $T < T_{\rm g}$.

7. Conclusion

The present work provides a methodology for the assessment of sealing failure with an application on SOFC sealings. In order to identify the physical mechanisms acting on an SOFC stack, in a first step, a full three-dimensional model has been analyzed. Three failure relevant mechanisms are determined resulting from (1) the inhomogeneous temperature field arising during operation (2) the pressure load caused by a weight on top of the stack and (3) the mismatch in thermal expansion coefficients of the layered materials steel and glass ceramics. After having identified these mechanisms, a reduced two-dimensional representative model is employed in order to investigate the crack initiation in the glass ceramics sealing. Depending on whether the present temperature is above or below the glass transition temperature, two different kinds of analysis are followed.

If the temperature is below the glass transition temperature, a linear elastic, brittle material behavior is presumed. For this case, a coupled stress and energy criterion within the framework of Finite Fracture Mechanics is proposed. The coupled criterion yields the critical temperature change and corresponding crack length. It indicates that the mismatch in thermal expansion coefficients (mechanism 3) dominates the failure occurrence in the case of linear elastic, brittle material behavior. Furthermore the coupled criterion revealed that the fracture toughness $\mathcal{G}_{I,c}$ is the most significant material parameter which must be determined properly in order to achieve a reliable result concerning the failure load.

In sections where the present temperature is above the glass transition temperature, viscoelastic material behavior is presumed. Performing viscoelastic calculations at the representative model led to the finding, that in this case the pressure load caused by the weight on or of the stack (mechanism 2) is dominant leading to very large deformations which may cause sealing failure.

Acknowledgement

The authors are grateful to the *Forschungszentrum Jülich* for financial support and good cooperation.

References

- P. Edwards, V. Kuznetsov, W. David, N. Brandon, Hydrogen and fuel cells: Towards a sustainable energy future, Energy Policy 36 (2008) 4356–4362.
- [2] A. B. Stambouli, E. Traversa, Fuel cells, an alternative to standard sources of energy, Renewable and Sustainable Energy Reviews 6 (2002) 295–304.
- [3] L. Carrette, K. A. Friedrich, U. Stimming, Fuel Cells Fundamentals and Applications, Fuel Cells 1 (2001) 5–39.
- [4] R. M. Ormerod, Solid oxide fuel cells, Chemical Society Reviews 32 (2003) 17–28.
- [5] A. B. Stambouli, E. Traversa, Solid oxide fuel cells (SOFCs): a review of an environmentally clean and efficient source of energy, Renewable and Sustainable Energy Reviews 6 (2002) 433–455.
- [6] V. Mehta, J. S. Cooper, Review and analysis of PEM fuel cell design and manufacturing, Journal of Power Sources 114 (2003) 32–53.
- [7] R. Othman, A. L. Dicks, Z. Zhu, Non precious metal catalysts for the PEM fuel cell cathode, International Journal of Hydrogen Energy 37 (2012) 357–372.
- [8] Y. Feng, N. Alonso-Vante, Nonprecious metal catalysts for the molecular oxygen-reduction reaction, physica status solidi (b) 245 (2008) 1792–1806.
- [9] X. Cheng, Z. Shi, N. Glass, L. Zhang, J. Zhang, D. Song, Z.-S. Liu, H. Wang, J. Shen, A review of PEM hydrogen fuel cell contamination: Impacts, mechanisms, and mitigation, Journal of Power Sources 165 (2007) 739–756.
- [10] O. Yamamoto, Solid oxide fuel cells: fundamental aspects and prospects, Electrochimica Acta 45 (2000) 2423–2435.
- [11] A. Weber, E. Ivers-Tiffée, Materials and concepts for solid oxide fuel cells (SOFCs) in stationary and mobile applications, Journal of Power Sources 127 (2004) 273–283.
- [12] N. Q. Minh, Solid oxide fuel cell technology?features and applications, Solid State Ionics 174 (2004) 271–277.
- [13] N. Q. Minh, Ceramic Fuel Cells, Journal of the American Ceramic Society 76 (1993) 563–588.

- [14] L. Blum, W. A. Meulenberg, H. Nabielek, R. Steinberger-Wilckens, Worldwide SOFC Technology Overview and Benchmark, International Journal of Applied Ceramic Technology 2 (2005) 482–492.
- [15] J. W. Fergus, Sealants for solid oxide fuel cells, Journal of Power Sources 147 (2005) 46–57.
- [16] M. Mahapatra, K. Lu, Seal glass for solid oxide fuel cells, Journal of Power Sources 195 (2010) 7129–7139.
- [17] M. Bram, S. Reckers, P. Drinovac, J. Mönch, R. W. Steinbrech, H. P. Buchkremer, D. Stöver, Deformation behavior and leakage tests of alternate sealing materials for SOFC stacks, Journal of Power Sources 138 (2004) 111–119.
- [18] P. A. Lessing, A review of sealing technologies applicable to solid oxide electrolysis cells, Journal of Materials Science 42 (2007) 3465– 3476.
- [19] Y.-S. Chou, J. W. Stevenson, L. A. Chick, Ultra-low leak rate of hybrid compressive mica seals for solid oxide fuel cells, Journal of Power Sources 112 (2002) 130–136.
- [20] Y.-S. Chou, J. W. Stevenson, Phlogopite mica-based compressive seals for solid oxide fuel cells: effect of mica thickness, Journal of Power Sources 124 (2003) 473–478.
- [21] Y.-S. Chou, J. W. Stevenson, Novel infiltrated Phlogopite mica compressive seals for solid oxide fuel cells, Journal of Power Sources 135 (2004) 72–78.
- [22] Y.-S. Chou, J. W. Stevenson, L. A. Chick, Novel Compressive Mica Seals with Metallic Interlayers for Solid Oxide Fuel Cell Applications, Journal of the American Ceramic Society 86 (2003) 1003–1007.
- [23] S. Le, K. Sun, N. Zhang, M. An, D. Zhou, J. Zhang, D. Li, Novel compressive seals for solid oxide fuel cells, Journal of Power Sources 161 (2006) 901–906.
- [24] S. P. Simner, J. W. Stevenson, Compressive mica seals for SOFC applications, Journal of Power Sources 102 (2001) 310–316.
- [25] F. Smeacetto, A. Chrysanthou, M. Salvo, T. Moskalewicz, F. D'Herin Bytner, L. Ajitdoss, M. Ferraris, Thermal cycling and ageing of a glass-ceramic sealant for planar SOFCs, International Journal of Hydrogen Energy 36 (2011) 11895–11903.
- [26] Z. Yang, J. W. Stevenson, K. D. Meinhardt, Chemical interactions of bariumâĂŞcalciumâĂŞaluminosilicate-based sealing glasses with oxidation resistant alloys, Solid State Ionics 160 (2003) 213–225.
- [27] P. Batfalsky, V. Haanappel, J. Malzbender, N. Menzler, V. Shemet, I. Vinke, R. Steinbrech, Chemical interaction between glassâĂŞceramic sealants and interconnect steels in SOFC stacks, Journal of Power Sources 155 (2006) 128–137.
- [28] F. Smeacetto, M. Salvo, M. Ferraris, J. Cho, A. Boccaccini, GlassâĂŞceramic seal to join Crofer 22 APU alloy to YSZ ceramic in planar SOFCs, Journal of the European Ceramic Society 28 (2008) 61–68.
- [29] K. L. Ley, M. Krumpelt, R. Kumar, J. H. Meiser, I. Bloom, Glass-ceramic sealants for solid oxide fuel cells: Part I. Physical properties, Journal of Materials Research 11 (1996) 1489–1493.
- [30] H.-T. Chang, C.-K. Lin, C.-K. Liu, High-temperature mechanical properties of a glass sealant for solid oxide fuel cell, Journal of Power Sources 189 (2009) 1093–1099.
- [31] J. Malzbender, J. Mönch, R. W. Steinbrech, T. Koppitz, S. M. Gross, J. Remmel, Symmetric shear test of glass-ceramic sealants at SOFC operation temperature, Journal of Materials Science 42 (2007) 6297– 6301.
- [32] E. Stephens, J. Vetrano, B. Koeppel, Y. Chou, X. Sun, M. Khaleel, Experimental characterization of glassâĂŞceramic seal properties and their constitutive implementation in solid oxide fuel cell stack models, Journal of Power Sources 193 (2009) 625–631.
- [33] J. Malzbender, Y. Zhao, Flexural Strength and Viscosity of Glass Ceramic Sealants for Solid Oxide Fuel Cell Stacks, Fuel Cells 12 (2012) 47–53.
- [34] C.-K. Lin, K.-L. Lin, J.-H. Yeh, W.-H. Shiu, C.-K. Liu, R.-Y. Lee, Aging effects on high-temperature creep properties of a solid oxide fuel cell glass-ceramic sealant, Journal of Power Sources 241 (2013) 12–19.
- [35] C.-K. Lin, T.-T. Chen, Y.-P. Chyou, L.-K. Chiang, Thermal stress

- analysis of a planar SOFC stack, Journal of Power Sources 164 (2007) 238–251
- [36] M. Peksen, A coupled 3D thermofluidâĂŞthermomechanical analysis of a planar type production scale SOFC stack, International Journal of Hydrogen Energy 36 (2011) 11914–11928.
- [37] L. Blum, S. M. Groß, J. Malzbender, U. Pabst, M. Peksen, R. Peters, I. C. Vinke, Investigation of solid oxide fuel cell sealing behavior under stack relevant conditions at Forschungszentrum Jülich, Journal of Power Sources 196 (2011) 7175–7181.
- [38] M. Peksen, 3D thermomechanical behaviour of solid oxide fuel cells operating in different environments, International Journal of Hydrogen Energy 38 (2013) 13408–13418.
- [39] D. Leguillon, Strength or toughness? A criterion for crack onset at a notch, European Journal of Mechanics - A/Solids 21 (2002) 61–72.
- [40] P. Weißgraeber, D. Leguillon, W. Becker, A review of Finite Fracture Mechanics: crack initiation at singular and non-singular stress raisers, Archive of Applied Mechanics 86 (2016) 375–401.
- [41] A. Nakajo, F. Mueller, J. Brouwer, J. Van herle, D. Favrat, Mechanical reliability and durability of SOFC stacks. Part I: Modelling of the effect of operating conditions and design alternatives on the reliability, International Journal of Hydrogen Energy 37 (2012) 9249–9268.
- [42] ThyssenKrupp, Crofer 22 APU Material Data Sheet No. 4046, 2010.
- [43] Y. Zhao, J. Malzbender, S. M. Gross, The effect of room temperature and high temperature exposure on the elastic modulus, hardness and fracture toughness of glass ceramic sealants for solid oxide fuel cells, Journal of the European Ceramic Society 31 (2011) 541–548.
- [44] B. C. Greven, Glass-Ceramic Sealant Reinforcement for High-Temperature Applications, Ph.D. thesis, 2014.
- [46] V. Hein, F. Erdogan, Stress singularities in a two-material wedge, International Journal of Fracture Mechanics 7 (1971) 317–330.
- [47] T. Kant, K. Swaminathan, Estimation of transverse/interlaminar stresses in laminated composites âĂŞ a selective review and survey of current developments 49 (2000) 65–75.
- [48] C. Mittelstedt, W. Becker, Interlaminar Stress Concentrations in Layered Structures: Part I A Selective Literature Survey on the Free-Edge Effect since 1967, Journal of Composite Materials 38 (2004) 1037–1062.
- [49] C. Mittelstedt, W. Becker, Fast and reliable analysis of free-edge stress fields in a thermally loaded composite strip by a layerwise laminate theory, International Journal for Numerical Methods in Engineering 67 (2006) 747–770.
- [50] M. Waddoups, J. Eisenmann, B. Kaminski, Macroscopic Fracture Mechanics of Advanced Composite Materials, Journal of Composite Materials 5 (1971) 446–454.
- [51] J. B. Leblond, P. Mouro, Crack propagation from a pre-existing flaw at a notch root. I. Introduction and general form of the stress intensity factors at the initial crack tip, International Journal of Fracture 104 (2000) 211–224.
- [52] J. B. Leblond, P. Mouro, Crack propagation from a pre-existing flaw at a notch root âĂŞ II: Detailed form of the stress intensity factors at the initial crack tip and conclusion., International Journal of Fracture 104 (2000) 225–239.
- [53] H. Neuber, Zur Theorie der Kerbwirkung bei Biegung und Schub, Ingenieur-Archiv 5 (1934) 238–244.
- [54] J. Whitney, R. Nuismer, Stress Fracture Criteria for Laminated Composites Containing Stress Concentrations, Journal of Composite Materials 8 (1974) 253–265.
- [55] D. Taylor, The theory of critical distances, Engineering Fracture Mechanics 75 (2008) 1696–1705.
- [56] M. L. Dunn, W. Suwito, S. Cunningham, Fracture initiation at sharp notches: Correlation using critical stress intensities, International Journal of Solids and Structures 34 (1997) 3873–3883.
- [57] Z. Qian, A. Akisanya, An experimental investigation of failure initiation in bonded joints, Acta Materialia 46 (1998) 4895–4904.
- [58] G. I. Barenblatt, The mathematical theory of equilibrium cracks in

- brittle fracture, Advances in Applied Mechanics 7 (1962) 55-129.
- [59] D. Dugdale, Yielding of steel sheets containing slits, Journal of the Mechanics and Physics of Solids 8 (1960) 100–104.
- [60] Z. Hashin, Finite thermoelastic fracture criterion with application to laminate cracking analysis, Journal of the Mechanics and Physics of Solids 44 (1996) 1129–1145.
- [61] E. Martin, D. Leguillon, N. Carrère, A twofold strength and toughness criterion for the onset of free-edge shear delamination in angle-ply laminates, International Journal of Solids and Structures 47 (2010) 1297–1305.
- [62] S. Dölling, J. Hahn, J. Felger, S. Bremm, W. Becker, A scaled boundary finite element method model for interlaminar failure in composite laminates, Composite Structures 241 (2020) 111865.
- [63] J. C. Brewer, P. A. Lagace, Quadratic Stress Criterion for Initiation of Delamination, Journal of Composite Materials 22 (1988) 1141–1155.
- [64] S. Ogihara, J. Koyanagi, Investigation of combined stress state failure criterion for glass fiber/epoxy interface by the cruciform specimen method, Composites Science and Technology 70 (2010) 143–150.
- [65] I. García, D. Leguillon, Mixed-mode crack initiation at a v-notch in presence of an adhesive joint, International Journal of Solids and Structures 49 (2012) 2138–2149.
- [66] V.-X. Tran, D. Leguillon, A. Krishnan, L. R. Xu, Interface crack initiation at V-notches along adhesive bonding in weakly bonded polymers subjected to mixed-mode loading, International Journal of Fracture 176 (2012) 65–79.
- [67] E. M. Wu, R. C. Reuter Jr., Crack Extension in Fiberglass Reinforced Plastics, Technical Report, Department of Theoretical and Applied Mechanics, University of Illinois, 1965. URL: https://apps.dtic. mil/sti/citations/AD0613576.
- [68] J. Reeder, An Evaluation of Mixed-Mode Delamination Failure Criteria, Technical Report, 1992. URL: https://ntrs.nasa.gov/citations/ 19920009705.
- [69] H. Abdoli, P. Alizadeh, D. Boccaccini, K. Agersted, Effects of thermal aging on thermo-mechanical behavior of a glass sealant for solid oxide cell applications, Journal of the European Ceramic Society 34 (2014) 2525–2534.
- [70] F. Greco, H. L. Frandsen, A. Nakajo, M. F. Madsen, J. Van herle, Modelling the impact of creep on the probability of failure of a solid oxide fuel cell stack, Journal of the European Ceramic Society 34 (2014) 2695–2704.
- [71] J. Malzbender, Y. Zhao, T. Beck, Fracture and creep of glassâĂŞceramic solid oxide fuel cell sealant materials, Journal of Power Sources 246 (2014) 574–580.
- [72] Y. Zhao, J. Malzbender, Elevated temperature effects on the mechanical properties of solid oxide fuel cell sealing materials, Journal of Power Sources 239 (2013) 500–504.
- [73] N. Stein, P. Weißgraeber, W. Becker, A model for brittle failure in adhesive lap joints of arbitrary joint configuration, Composite Structures 133 (2015) 707–718.
- [74] L. F. M. da Silva, T. N. S. S. Rodrigues, M. A. V. Figueiredo, M. F. S. F. de Moura, J. A. G. Chousal, Effect of Adhesive Type and Thickness on the Lap Shear Strength, The Journal of Adhesion 82 (2006) 1091–1115.
- [75] R. Campilho, M. de Moura, J. Domingues, Numerical prediction on the tensile residual strength of repaired CFRP under different geometric changes, International Journal of Adhesion and Adhesives 29 (2009) 195–205.
- [76] M. Jung Lee, T. Min Cho, W. Seock Kim, B. Chai Lee, J. Ju Lee, Determination of cohesive parameters for a mixed-mode cohesive zone model, International Journal of Adhesion and Adhesives 30 (2010) 322–328.
- [77] H. Abdoli, P. Alizadeh, D. Boccaccini, K. Agersted, Fracture toughness of glass sealants for solid oxide fuel cell application, Materials Letters 115 (2014) 75–78.
- [78] J. Malzbender, R. W. Steinbrech, L. Singheiser, Determination of the interfacial fracture energies of cathodes and glass ceramic sealants in a planar solid-oxide fuel cell design, Journal of Materials Research 18 (2003) 929–934.

Page 13 of 14

- [79] J. Malzbender, R. W. Steinbrech, L. Singheiser, P. Batfalsky, Fracture Energies of Brittle Sealants for Planar Solid Oxide Fuel Cells, in: N. P. Bansal (Ed.), Advances in Solid Oxide Fuel Cells: Ceramic Engineering and Science Proceedings, 2008, pp. 285–291.
- [80] R. D. Adams, N. A. Peppiatt, Stress analysis of adhesive-bonded lap joints, Journal of Strain Analysis 9 (1974) 185–196.
- [81] A. Objois, Y. Gilibert, B. Fargette, Theoretical and Experimental Analysis of the Scarf Joint Bonded Structure: Influence of the Adhesive Thickness on the Micro-mechanical Behavior, The Journal of Adhesion 70 (1999) 13–32.
- [82] D. M. Gleich, M. J. L. Van Tooren, A. Beukers, Analysis and evaluation of bondline thickness effects on failure load in adhesively bonded structures, Journal of Adhesion Science and Technology 15 (2001) 1091–1101.